Research Square

Preprints are preliminary reports that have not undergone peer review.
They should not be considered conclusive, used to inform clinical practice,
or referenced by the media as validated information.

Design and Simulation of a Wideband Bridged-Cavity SIW-DRA for D-Band Frequency Applications

Emmanuel K. Chemweno

ce_kiprop@yahoo.co.uk

Moi University

Pradeep Kumar

University of KwaZulu-Natal

Thomas J. O. Afullo

University of KwaZulu-Natal

Article

Keywords:

Posted Date: November 23rd, 2026

DOI: https://doi.org/10.21203/rs.3.rs-11362205/v1

License: This work is licensed under a Creative Commons Attribution 4.0 International License.
Read Full License

Additional Declarations: No competing interests reported.

Design and Simulation of a Wideband Bridged-Cavity SIW-DRA for D-Band Frequency Applications

Emmanuel K. Chemweno[1*], Pradeep Kumar[2†] and Thomas J. O. Afullo[2†]

[1*]Department of Electrical and electronics engineering, Moi University, , Eldoret, Kenya.
[2]Discipline of Electrical, Electronic and Computer Engineering, University of KwaZulu-Natal, Howard College Campus, Durban, South Africa.

*Corresponding author(s). E-mail(s): ce_kiprop@yahoo.co.uk;
Contributing authors: pkumar_123@yahoo.com; afullot@ukzn.ac.za;
†These authors contributed equally to this work.

Abstract

A novel bridge-cavity SIW-DRA feed structure is proposed. The dimensions or the DRA are chosen to ensure higher mode operation of the DR element. The DR is excited through two slots fed from dissimilar SIW cavities. Simulation results show wideband range of 130.17 GHz - 170.6 GHz, representing a -10 dB impedance bandwidth of 26.8% at a centre frequency of 150.34 GHz. Radiation pattern show stable broadside radiation patterns, with a peak gain performance of 8.87 dBi and a maximum efficiency of 77.8%. The wideband operation, broadside patterns, relatively stable gain and efficiency demonstrates the suitability of the proposed antenna structure for wideband millimeter and sub-Terahertz applications, where the different resonances may be exploited for different operating channels.

Keywords: Dielectric Resonator Antenna (DRA) , Millimeter (mm) Waves , Substrate Integrated Waveguide , Terahertz (THz)

1 Introduction

High-speed wireless communication networks are necessary to provide high data rates required to support the emerging internet of things (IoT) based broadband wireless applications and services. Consequently, there is need for designs of reliable wireless systems operating in the millimeter (mm) and terahertz (THz) frequency spectrum. The D-band constitutes the sub-THz frequencies that is under exploration for possible exploitation for applications such as wireless high-speed device-to-device communications and backhaul links [1]. This band is characterized by large bandwidth (110 - 170 GHz) and high data speeds of up to 100 Gb/s [2].

At frequencies above 100 GHz, there are challenges of increased path losses and signal attenuation due to atmospheric absorption. These limit the range of communications leading to short propagation distances. To maintain reliable communication, these effects can be mitigated by use of efficient, high-gain and directional antennas [3]. Different antenna topologies have been proposed for application in this frequency band. These include horn antennas [4], package based antennas [1], [5], [6], microstrip patch antennas (MPAs) [7], substrate integrated waveguide (SIW) slot antennas [8], dielectric resonator antennas (DRAs) [9], magneto-electric (ME) dipoles [10] among others. In this research, we present a novel structure for a wideband SIW-DRA operating between 130 - 170 GHz. In the proposed design, two dissimilar SIW cavities simultaneously excite a dielectric resonator (DR) element that forms a bridge across the cavities.

This work is organized as follows: Section 2 provides a review of the various designs for D-band antennas. Section 3 presents the design structure of the proposed bridged-cavity SIW-DRA. Results and analysis of the proposed antenna are presented in section 4. Finally, section 5 provides the conclusion of this work.

2 Related Works

A high-gain D-Band integrated SIW-fed metallic horn antenna is proposed in [4]. The antenna is realized by assembling a metallic horn with a SIW feed line. A peak gain of 15.46 dBi and a -10 dB bandwidth of 18.9% (129.5–156.5 GHz) is achieved. This antenna design suffers the disadvantage being bulky which renders it difficult to be directly integrated with planar circuits. From the perspective of low profile, package-based antennas are attractive. Package-based antennas can broadly be categorized as on chip antennas (OCA) and antenna-in-package (AiP) antennas. These antennas have the attributes of being low in profile with radiating elements taking different forms such as dipoles, printed Yagi, on-chip DRA, MPA, ME dipoles etc. An on-chip folded antenna is reported in [5], designed to operate at 165-175 GHz, yielding a gain of 5 dBi with a maximum efficiency of 45%. An AiP based quasi-Yagi antenna is proposed [1]. The antenna operates in the entire D-band and achieves 3.16 - 5.9 dBi peak gain across the entire band. A half-mode SIW (HMSIW) cavity backed on-chip DRA is proposed in [6]. The DRA is excited for higher-order mode operation to achieve a bandwidth of 7% and gain of 7.5 dBi at 135 GHz. Package-based antennas allow for integration and low interconnect losses between the antenna, monolithic millimeter-wave integrated circuit (MMIC) and other active RF components. However, the major limitations of

silicon-based on-chip antennas is that they radiate inefficiently and suffer from very poor gain and directivity [5].

A wideband SIW-based slot antenna is presented in [8]. The antenna is designed on standard PCB. An impedance bandwidth of 42.86% was achieved using multiple high-order modes of the SIW-fed slot with a peak gain of 10.8 dBi. A dual-band SIW cavity-backed slot antenna radiating at 146.6 GHz and 167.2 GHz is presented in [11]. The -10 dB impedance bandwidths are above 3% across both bands with the maximum realized gains of 8.73 dBi and 9.29 dBi in the lower and upper bands respectively. Despite the design presented in [8] having a wide bandwidth, it is fed by a conventional waveguide making it not feasible for intergration with other front end devices.

A printed D-band patch antenna array on a quartz substrate is reported in [7]. The proposed design is designed to operate at 146 GHz with a single element antenna exhibiting a gain of 6.6 dBi and an impedance bandwidth of 6.6%. MPAs have the advantages of being low profile, easy to integrate and low cost due to less manufacturing complexity. At low frequencies, MPAs and MPA arrays become appropriate options when trade-offs between performance and feasibility are considered. However, at high frequencies, MPAs suffer severe ohmic losses, narrow bandwidth and surface waves leading to poor radiation efficiencies [12]. DRAs offer suitable alternatives because they can overcome the limitations associated with metallic antennas, *viz:* less conductive losses and high radiation efficiencies at high frequencies. DRAs are made from high-permittivity and low-loss ceramics materials. Their inherent attributes of low-profile, light weight, large bandwidth, high radiation efficiency and simple coupling schemes to commonly used transmission lines make them attractive for high frequency applications. In addition, different radiation characteristics can be achieved through the excitation of different radiation modes [13]. A wideband SIW-DRA with a peak gain of 11.67 dBi and bandwidth of 20.39% has been proposed for application in D-band [14].

Despite DRA offering better bandwidth performance compared to the MPA owing to its larger effective aperture, it still suffers the problem of narrow bandwidth [15]. Various techniques have been proposed to enhance the bandwidth performance of the DR-based antennas. These may be broadly categorized as techniques involving the modification of the DR element, incorporation of additional structures, adopting different feed configurations or those that involve modal excitation of the resonator among others [14], [16]. At mm-wave frequencies, the size of the DR element is small in size, with dimensions in the order of $\lambda_0/\sqrt{\epsilon_r}$. Techniques involving the modification of the DR element to create perforations and fractal geometries and those involving additional structures such as stacking and use of superstrates become unattractive owing to manufacturing tolerances [17] and increased structural complexities, respectively. An alternative approach is to excite two or more modes in a DRA so as to exhibit multiple resonances. In this manner, the DRA operates in higher order modes. Adjacent resonances are merged together to achieve a wideband operation provided that the radiation patterns of the individual modes are similar [16]. In addition, conventional feeding lines such as microstrips and coplanar feeds suffer high radiation losses. At high frequencies, the SIW feeds and interconnects can minimize the radiation losses

and parasitic radiation associated with microstrip feeds, thus providing a convenient way for excitation of the DR element [18].

3 Antenna Design

The geometry of the proposed bridged-cavity SIW-DRA antenna is shown in Fig. 1. The antenna consists of a high permittivity DR element placed on top of a two dissimilar SIW feeding cavities fed from the same source. Two lateral slots simultaneously excite the DR element to create radiation fields. The design of the antenna involves the designs of the DR element, the feed network and the application of impedance matching techniques for bandwidth improvement.

3.1 Dielectric resonator element design

A rectangular DR element made from 99.5% Alumina dielectric material of relative permittivity ϵ_{rd} =9.9 is selected as the radiating element. The rectangular-shaped DR has the advantage that different modes can be obtained from different choices of resonator dimensions L_{dra}, W_{dra} and H_{dra}. Consequently, the aspect rations of the DR (height/length and width/length) can be selected to provide a better bandwidth control [13], [19]. These dimensions are also selected to ensure that the DRA operates in higher order modes.

The resonant frequencies of the various modes can be predicted using the dielectric waveguide model (DWM) by solving the transcendental equations (1)-(3), given by [20]:

$$k_x \tan\left(\frac{k_x L_{dra}}{2}\right) = \sqrt{(\epsilon_{rd}-1)\,k_{0,mn}^2 - k_x^2} \tag{1}$$

$k_y = \frac{m\pi}{W_{dra}}$ and $k_z = \frac{n\pi}{2H_{dra}}$ are wavenumbers in the y- and z-directions which must satisfy the separation equation:

$$k_x^2 + k_y^2 + k_z^2 = \epsilon_{rd} k_{0,mn}^2 \tag{2}$$

Equation (2) is solved to determine the resonant frequencies for different DR modes using:

$$k_{0,mn} = \frac{2\pi f_{0,mn}}{c} \tag{3}$$

The DWM can be used to calculate the resonant frequencies of the various modes. However, some modes are degenerate and cannot be properly excited. The actual excited modes depend on feeding source and position, effects of the ground plane etc.

3.2 Design of the SIW feeding cavity

Fig. 1 (a) & (b) show the geometry of the top and bottom views of the SIW feed. The feed consists of two disimmilar SIW cavities designed from a low-loss RT Duroid 5880 substrate material of relative permittivity ϵ_r =2.2, loss tangent $\tan\delta$ =0.0009 and substrate thickness h =0.254 mm. Rows of equally spaced cylindrical metal via form

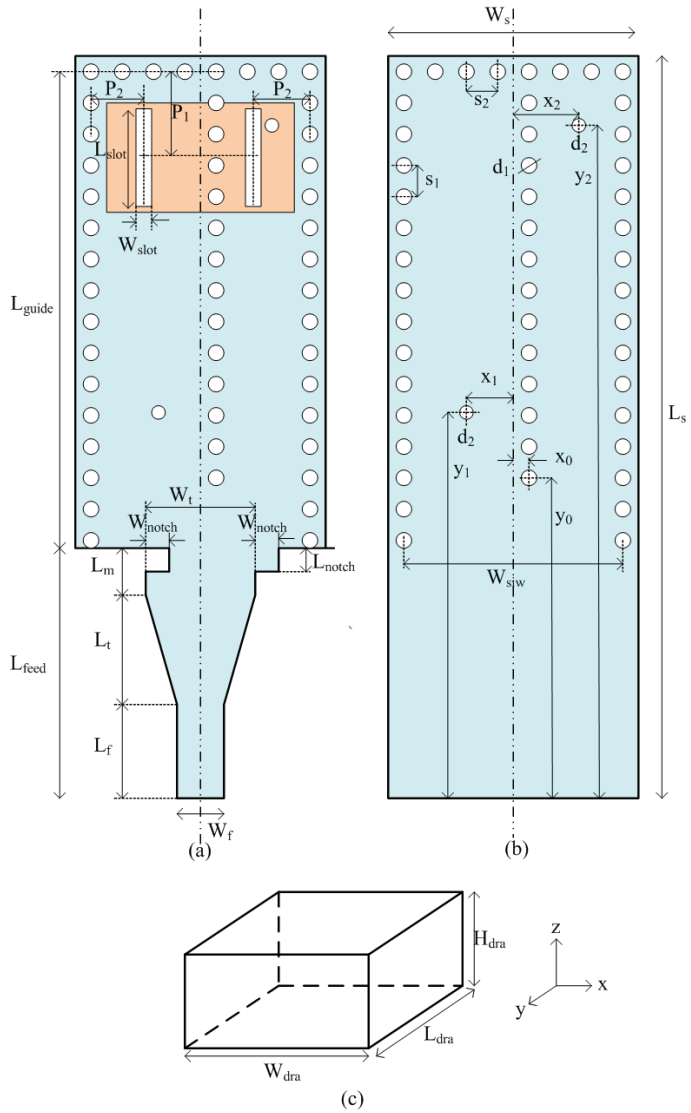


Fig. 1 Geometry of the proposed bridged-cavity SIW-DRA showing (a) top view, (b) bottom view and (c) DR element

the walls of the SIW cavities of via-to-via widths of $W_{siw}/2 + x_0$ and $W_{siw}/2 - x_0$, where W_{siw} is the via-to-via width of the entire structure as depicted in the figure. The cavities are fed from a stepped microstrip feed line centrally placed with respect to the entire antenna structure. The stepped microstrip line matches the input impedance of a 50Ω microstrip feed line of width W_f to the cavity structure through a tapered transition section. An asymmetrical notch is introduced on the feed for improved impedance matching. The cavities are terminated at equal distance L_{guide} from the feeding end using a fence equally spaced via to form cavity resonators. Two equal slots,

one on each cavity are etched on the upper conductor of the cavity at distances P_1 from the terminating via and P_2 from the extreme walls of the cavities. Two inductive via of diameter d_2 are embedded on the feed cavity structure at points (x_1, y_1) and (x_2, y_2) for impedance matching. Finally, the rectangular DR element is placed on top of the cavity structure and is excited from the cavities through the rectangular slots beneath it as shown in Fig. 1.

The SIW emulates a dielectric-filled waveguide whose lateral walls are formed by rows of equally spaced vias. In the design of the SIW, the via diameter d and pitch (spacing) s must be carefully selected so as to minimize radiation leakage along the walls of the SIW. This is satisfied by observing the rules given in [21] given by equations 4 (a) & (b).

$$d < \lambda_g/5 \tag{4a}$$

$$s \leq 2d \tag{4b}$$

Where λ_g is the guided wavelength.

The via-to-via width of the SIW is determined by mapping the dimensions of a conventional rectangular metallic waveguide of dimension a and b, $(a > b)$ to achieve the same cut-off frequency f_c at the lowest TE_{10} mode. For a SIW operating in TE_{10} propagating mode, the design procedure and equations given in [22] are applied.

$$f_{c_{mn}} = \frac{c}{2\pi\sqrt{\varepsilon_r}}\sqrt{\left(\frac{m\pi}{a}\right)^2 + \left(\frac{n\pi}{b}\right)^2} \tag{5}$$

$$a = \frac{c}{2f_{c_{10}}\sqrt{\varepsilon_r}} \tag{6}$$

$$a = W_{siw} - 1.08\frac{d^2}{s} + 0.1\frac{d^2}{W_{siw}} \tag{7}$$

$$\lambda_{g10} = 2\pi/\sqrt{\left(\frac{\varepsilon_r\omega^2}{c^2}\right) - \left(\frac{\pi}{a}\right)^2} \tag{8}$$

where c is the speed of light, ε_r the relative permittivity of the dielectric material filling the waveguide, W_{siw} is the via-to-via width of the SIW and m, n are the mode indices.

Equations (5)-(8) are based on the dominant propagating modes of the SIW. Wide operating bandwidths can be achieved by higher-order cavity modes while maintaining the design sizes of the via diameter and pitch.

3.3 Impedance matching and bandwidth enhancement

Two key design approaches have been employed in the proposed design: excitation of higher order modes and modification of the feeding arrangements. First, the dimensions of the DR element were chosen to allow the excitation of fundamental and higher order modes. Secondly, since the actual modes excited depend on the feeding source

and its position, a novel feed structure is proposed. These two techniques when used independently or applied together often gives rise to a multi-band antenna response. The adjacent bands are merged together to achieve a wideband response. Two inductive metal via together with an asymmetrical notch on the stepped microstrip feed are employed to merge together the passbands and enhance the bandwidth of the proposed design.

The proposed antenna is modeled and simulated using CST Microwave Studio. The antenna dimensional parameters are optimized for better performance. Table 1 shows the optimized antenna parameters.

Table 1 Dimensional parameters of the proposed bridged cavity SIW-DRA antenna

Parameter	Description	Value
d_1	SIW via diameter	0.3
d_2	Inductive via diameter	0.28
h_{copper}	Copper thickness	0.017
h_{sub}	Substrate height	0.254
H_{dra}	Dielectric resonator height	1.6
L_{dra}	Dielectric resonator length	1.98
L_f	50Ω microstrip feed length	0.65
L_{feed}	Microstrip transition section length	1.76
L_{guide}	SIW resonator length	8.55
L_m	Stepped section length	0.35
L_{notch}	Notch length	0.2
L_s	Substrate length	10.61
L_{slot}	Slot length	1.8
L_t	Tapered section length	0.76
P_1	Slot position from terminating via	1.53
P_2	Slot position from SIW wall	0.94
s_1	Lateral via pitch	0.56
s_2	Terminating via pitch	0.54
W_{dra}	Dielectric resonator width	3.3
W_f	Feed width	0.67
W_{notch}	Notch width	0.15
W_s	Substrate width	4.38
W_{siw}	Via-to-via width of the antenna	3.78
W_{slot}	Slot width	0.35
W_t	Tapered transition width	0.96
x_0	x-position of common SIW wall	0.27
x_1	x-position of inductive Via 1	0.76
x_2	x-position of inductive Via 2	1.31
y_0	x-position of common SIW wall	3.04
y_1	y-position of inductive Via 1	4.14
y_2	y-position of inductive Via 2	9.27

All dimensions in mm

4 Antenna simulation, results and analysis

Bandwidth performance

The simulated reflection coefficients of the proposed bridged-cavity SIW-DRA is shown in Fig. 2. The s_{11} curve exhibits multiple resonances whose passbands merge together to achieve a wideband response. The proposed design shows a frequency of operation between 130.17 - 170.6 GHz. This represents a -10 dB impedance bandwidth of 26.8%.

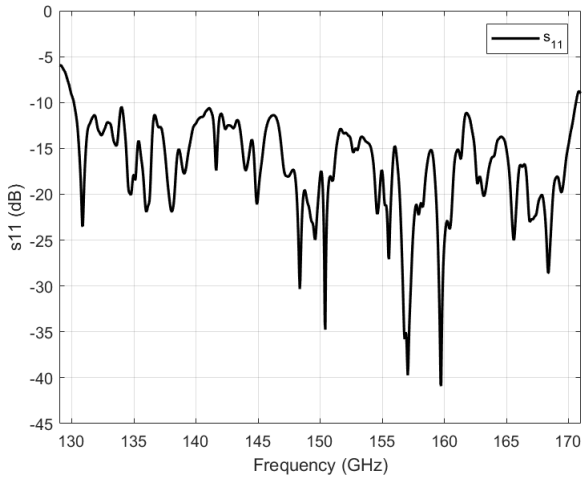


Fig. 2 Simulated reflection coefficients of the proposed SIW-DRA.

The feed cavity excites multiple higher-order modes in the resonator with each mode corresponding to unique resonance frequency. Several feeding arrangements have been reported in literature for bandwidth enhancement of SIW cavity-fed DRAs. These techniques generally focus on the modification of the feeding apertures and cavities. These include the use of double slots, meander slots, cross slots, U-shaped slots, . These modifications excite higher-order modes and induce additional resonances which are desirably combined to achieve a broadband response.

This work presents a novel feeding structure for excitation of multiple resonances in a DRA. The proposed design involves the use of two cavities to simultaneously excite multiple modes in a DR. Input electromagnetic energy is split and fed to the SIW cavities, which in turn excite the DR through coupling slots. From the simulation results, a broad bandwidth of 26.8% is achieved, thus demonstrating that the proposed bridged-cavity structure offer designers flexible design approaches for DRA bandwidth enhancement. Simulations show that each cavity can independently be optimized.

Antenna evolution and impedance matching

When adjacent resonances due to higher-order modes are sufficiently close, the bands merge together to enhance the antenna bandwidth. Often, this may not be achieved

and it becomes necessary to apply impedance matching techniques to minimize the mismatch in the stop bands. In the proposed design, three impedance matching techniques are employed: application of inductive metal via and the application of an asymmetrical notch and a patch on the SIW feed.

The sequential application of this techniques give rise to different antenna configurations. In order to investigate the contribution of the various techniques, we label the different configurations as follows:

Antenna 1 - Bridged-cavity SIW-DRA
Antenna 2 - Bridged-cavity SIW-DRA with embedded inductive metal via
Antenna 3 - Bridged-cavity SIW-DRA with embedded inductive metal via and an asymmetrical notch
Antenna 4 - Bridged-cavity SIW-DRA with embedded inductive metal via with both an asymmetrical notch and patch

Fig. 3 shows the reflection coefficients and input impedance of the different antenna configurations. For brevity, only the reactive impedance is shown.

Fig. 3 (a) presents the s_{11} and Im z_{in} for Antenna 1. It is observed that Antenna 1 suffers severe input impedance mismatch in the (130.7-136.0) GHz, (142.9-147.0) GHz, (151.3-152.6) GHz and (160.6-167.3) GHz frequency bands as highlighted in the figure. Reflections in these bands can be minimized through the use of reactive elements in the SIW.

From the impedance plot of the Fig. 3 (a), the antenna input reactance is not zero. Specifically, the mismatch in (130.7-136.0) GHz and (160.6-167.3) GHz bands is associated to capacitive input reactance while for bands (142.9-147.0) GHz and (151.3-152.6) GHz, the input reactance is inductive.

In this work, we propose the use of inductive vias to minimize the input reactance of Antenna 1. Inductive vias introduces discontinuities in waveguides and are useful for impedance matching. The discontinuities give rise to a reflect waves and a storage of reactive energy in the vicinity of the discontinuities because of excitation of higher order waveguide modes which are evanescent [23]. By properly positioning the vias, significant impedance matching is achieved.

Fig. 3 (b) compares the simulation results for Antennas 1 and 2. The simulation results show that metal vias introduce inductive reactance to minimizes the input capacitive reactance. This results in improved s_{11} performance as highlighted in the figure. This improves the impedance matching in the targeted band without significantly deteriorating the the performance at other frequencies. However, Antenna 2 still exhibits a poor performance around the frequencies of 136.7 GHz and 146.4 GHz. By use of an asymmetrical notch on the SIW feed, some junction capacitance is introduced in Antenna 3 which causes improved impedance matching in these frequencies as shown in Fig. 3 (c). Further improvements in the impedance matching is achieved by extending the asymmetry in the feeding by use of a small patch depicted in Fig. 3 (d).

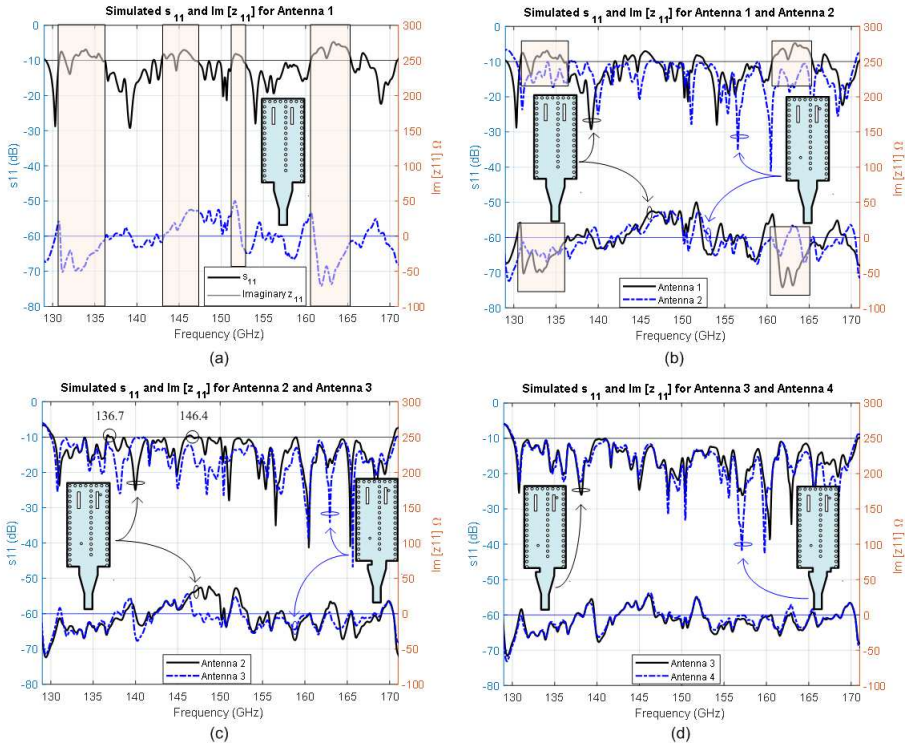


Fig. 3 Graphs showing the s_{11} performance and the input reactive impedance (z_{in}) for the different antenna configurations.

Radiation characteristics

The proposed bridged-cavity SIW-DRA exhibits multiple resonances within the D-band, indicating the excitation of higher-order in the DRA. The resonances occur at 130.85 GHz, 148.4 GHz, 150.4 GHz, 157.11 GHz, 159.8 GHz and 168.4 GHz. Each of this resonance corresponds to a different mode with unique field distribution and radiation characteristics. In this paper, the simulated E-plane and H-plane radiation patterns of the proposed bridged-cavity SIW-DRA for 130.85 GHz, 150.4 GHz and 168.4 GHz are displayed in Fig. 4. These frequencies are selected to represent the low, mid and high frequencies of the antenna operation.

From Fig. 4, it can be observed that the proposed antenna structure generally maintains broadside radiation patterns in both E-plane and H-plane at different resonant frequencies. The beam shapes and side-lobes vary, indicating that the radiation distribution is non-uniform. Despite these, the radiation of the main lobes at 130.85 GHz, 150.4 GHz and 168.4 GHz are concentrated around the upper hemisphere. This variation is expected because a DRA has mode-dependent radiation characteristics: different resonant modes produce different field distributions, thus different far-field radiation characteristics.

The wideband operation of the proposed structure is achieved by merging together adjacent resonances associated to the excited higher-order modes. Table 2 summarizes

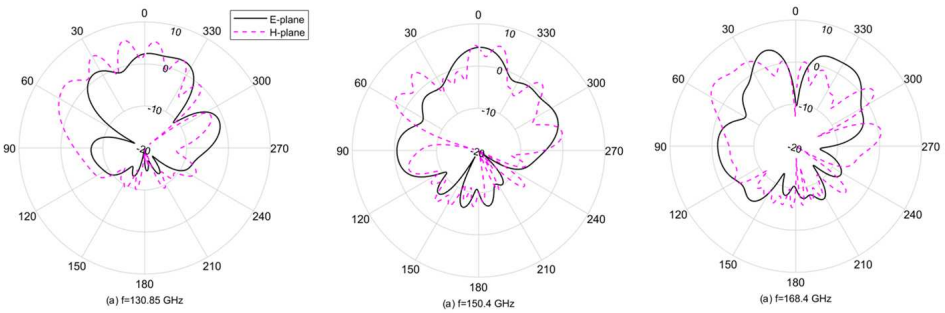


Fig. 4 Simulated E-plane and H-plane radiation patterns for the proposed bridged-cavity SIW-DRA at 130.85 GHz, 150.4 GHz and 168.4 GHz

the antenna radiation characteristics at 130.85 GHz, 148.4 GHz, 150.4 GHz, 157.11 GHz, 159.8 GHz and 168.4 GHz resonant frequencies. It is observed that the dominant radiation for each mode is in the broadside direction. This implies that the radiation pattern corresponding to the excited DR modes are similar, therefore, the antenna performance is not significantly degraded [16].

Table 2 Simulated radiation characteristics of the proposed bridged-cavity SIW-DRA

E-plane						
f (GHz)	130.85	148.4	150.4	157.11	159.8	168.4
Main Lobe Magnitude (dBi)	2.74	5.29	4.42	2.07	4.76	3.83
Main Lobe Direction	23.0^o	26.0^o	1.0^o	23.0^o	41.0^o	18.0^o
Angular width (3dB)	48.5^o	27.3^o	31.7^o	25.9^o	24.2^o	21.8^o
Side Lobe Level (dB)	-1.4	-2.1	-4.2	-2.1	-2.2	-1.0
H-plane						
Main Lobe Magnitude (dBi)	6.04	3.23	5.19	6.86	4.16	4.45
Main Lobe Direction	11.0^o	3.0^o	12.0^o	32.0^o	47.0^o	52.0^o
Angular width (3dB)	10.8^o	9.1^o	24.0^o	12.9^o	11.6	41.5^o
Side Lobe Level (dB)	-0.7	-0.8	-1.2	-1.6	-0.7	-1.7

Antenna gain and efficiency

The simulated gain and efficiency performance of the antenna is shown in Fig. 5. It can be observed that the antenna gain exhibits several peaks across the frequency band of operation, with a maximum gain of 8.87 dBi occuring at 146 GHz and 164 GHz. These variations are associated with the different modes excitations. However, the gain remains above approximately 5 dBi, indicating that the antenna maintains useful directional radiation over a broad frequency range.

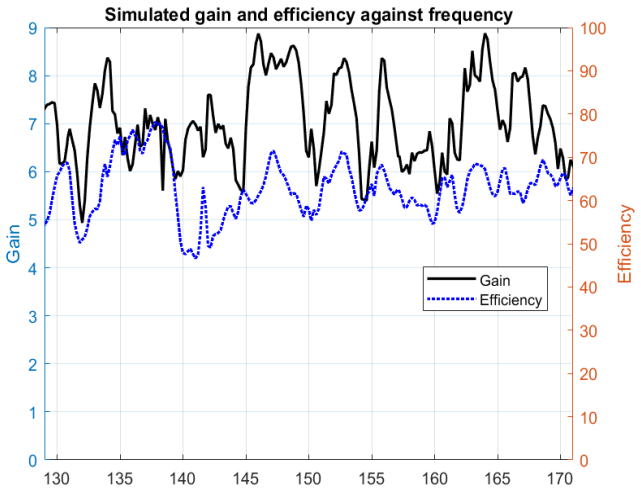


Fig. 5 Simulated gain and efficiency of the proposed bridged-cavity SIW-DRA

The proposed design exhibits an efficiency above 50% throughout the operating frequency band, with a peak of 77.8% at 132.8 GHz. The moderate-to-high efficiency indicate that the antenna converts the accepted input power into radiated electromagnetic energy effectively.

Overally, the proposed bridged-cavity structure exhibits relatively stable gain and efficiency across the operating frequencies.

Design validation

To validate the proposed bridge-cavity SIW-DRA, the optimized antenna was modelled and simulated using Ansys HFSS software. The computational techniques employed by these electromagnetic simulators are different, thus one can be independently used to validate the other.

Fig. 6 compares the s_{11} performance of the proposed designs in CST and HFSS environments. It is observed that there is a slight increase in the cut-off frequency from 130.17 Ghz to 132.1 GHz in the lower frequency band, while the upper cut-off remains unchanged. This causes a change in the impedance bandwidth from 28.8% to 25.5%. This change represents a modest reduction that does not significantly affect the bandwidth performance.

From Fig. 6, it is observed that the CST and HFSS simulators predict similar or close resonant frequencies. However, the magnitudes of the reflection coefficient at these resonances significantly vary depending on the computational approach used. There is close agreement in both the bandwidth performance and close resonances predicting similar mode excitation.

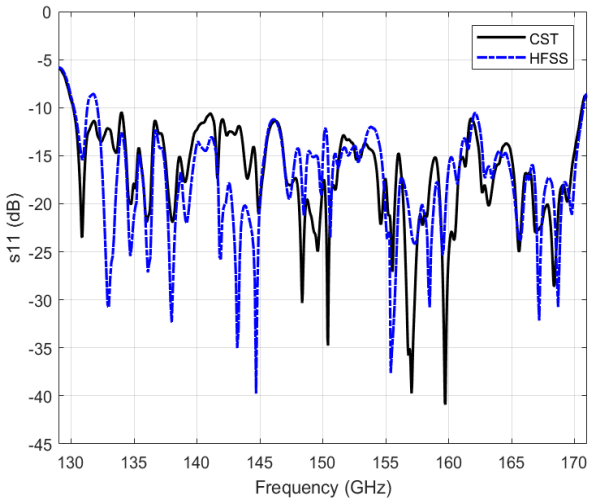


Fig. 6 Simulated s_{11} performance of bridged-cavity SIW-DRA using CST and HFSS.

5 Conclusion

In this work, a novel bridge-cavity SIW-DRA feed structure has been presented. Techniques incorporating use of twin apertures to excite the DR element have been reported in literature. The novelty of this work is the feeding of a DR element from dissimilar SIW cavities to excite various modes in the DR element. By employing impedance matching techniques, adjacent resonances can be merged to achieve a wide-band antenna operation for D-band applications. Simulations shows that the proposed structure achieves a wideband operation of 26.8% fractional impedance bandwidth centred at 150.34 GHz. The proposed antenna structure also exhibits stable broadside radiation, a peak gain of 8.87 dBi, and a maximum radiation efficiency of 77.8% across the operating band. These results confirm the suitability of the antenna structure for wideband millimeter-wave and sub-terahertz wireless communication systems, where its multiple resonances can be exploited to support different operating channels.

Declarations

- Data availability:
  The datasets generated and analysed during the current study are not publicly available because they constitute design and simulation data for which the article is under peer review, but are available from the corresponding author on reasonable request.

References

[1] Erdogan, S., Moon, K.-S.J., Kathaperumal, M., Swaminathan, M.: D-band integrated and miniaturized quasi-yagi antenna array in glass interposer. IEEE Transactions on Terahertz Science and Technology **13**(3), 270–279 (2023)

[2] Jia, X., Li, X., Erdogan, S., Moon, K.-S., Kim, J.W., Huang, K.-Q., Jordan, M.B., Swaminathan, M.: Antenna with embedded die in glass interposer for 6g wireless applications. IEEE Transactions on Components, Packaging and Manufacturing Technology **13**(2), 219–229 (2023)

[3] Nissanov, U., Singh, G., Kumar, N.: High gain microstrip array antenna with siw and fss for beyond 5 g at thz band. Optik **236**, 166568 (2021)

[4] Ma, C., Ma, S., Dai, L., Zhang, Q., Wang, H., Yu, H.: Wideband and high-gain d-band antennas for next-generation short-distance wireless communication chips. IEEE Transactions on Antennas and Propagation **69**(7), 3700–3708 (2020)

[5] Ahmad, W., Kucharski, M., Di Serio, A., Ng, H., Waldschmidt, C., Kissinger, D.: Planar highly efficient high-gain 165 GHz on-chip antennas for integrated radar sensors. IEEE Antennas Wirel Propag Lett 18 (11): 2429–2433 (2019)

[6] Hou, D., Hong, W., Goh, W.-L., Chen, J., Xiong, Y.-Z., Hu, S., Madihian, M.: D-band on-chip higher-order-mode dielectric-resonator antennas fed by half-mode cavity in cmos technology. IEEE Antennas and Propagation Magazine **56**(3), 80–89 (2014)

[7] Zhou, L., Tang, M., Gao, Z., Mao, J., Yue, H., Tang, Y.: Design and fabrication of patch antenna array on quartz glass substrate at 146 ghz. In: 2020 International Conference on Microwave and Millimeter Wave Technology (ICMMT), pp. 1–3 (2020). IEEE

[8] Altaf, A., Abbas, W., Seo, M.: A wideband siw-based slot antenna for *d*-band applications. IEEE Antennas and Wireless Propagation Letters **20**(10), 1868–1872 (2021)

[9] Chemweno, E.K., Kumar, P., Afullo, T.J.: Substrate integrated waveguide-dielectric resonator antenna for future wireless communication. SAIEE Africa Research Journal **113**(3), 119–128 (2022)

[10] Xu, Y., Wen, S., Dong, Y.: A d-band magneto-electric dipole antenna array based on ltcc technology. In: 2021 IEEE International Workshop on Electromagnetics: Applications and Student Innovation Competition (iWEM), pp. 1–3 (2021). IEEE

[11] Wang, D., Xu, K.-D.: Dual-band substrate integrated waveguide cavity-backed antenna based on ltcc in d-band. In: 2022 International Applied Computational Electromagnetics Society Symposium (ACES-China), pp. 1–3 (2022). IEEE

[12] Katoch, K., Singh, G.: Highly directive dielectric resonator rod array antenna at terahertz frequency for imaging applications. In: 2017 Fourth International Conference on Image Information Processing (ICIIP), pp. 1–6 (2017). IEEE

[13] Mongia, R.K., Bhartia, P.: Dielectric resonator antennas—a review and general design relations for resonant frequency and bandwidth. International Journal of Microwave and Millimeter-Wave Computer-Aided Engineering **4**(3), 230–247 (1994)

[14] Chemweno, E., Kumar, P., Afullo, T.: Design of high-gain wideband substrate integrated waveguide dielectric resonator antenna for d-band applications. Optik **272**, 170261 (2023)

[15] Chang, T.-H., Kiang, J.-F.: Bandwidth broadening of dielectric resonator antenna by merging adjacent bands. IEEE Transactions on Antennas and Propagation **57**(10), 3316–3320 (2009)

[16] Petosa, A., Ittipiboon, A.: Dielectric resonator antennas: A historical review and the current state of the art. IEEE antennas and Propagation Magazine **52**(5), 91–116 (2010)

[17] Xu, J., Chen, Z.N., Qing, X., Hong, W.: A single-layer siw slot array antenna with te 20 mode. In: Asia-Pacific Microwave Conference 2011, pp. 1330–1333 (2011). IEEE

[18] Wahab, W.M.A., Busuioc, D., Safavi-Naeini, S.: Low cost planar waveguide technology-based dielectric resonator antenna (dra) for millimeter-wave applications: Analysis, design, and fabrication. IEEE Transactions on Antennas and Propagation **58**(8), 2499–2507 (2010)

[19] Mongia, R.K., Ittipiboon, A.: Theoretical and experimental investigations on rectangular dielectric resonator antennas. IEEE Transactions on antennas and propagation **45**(9), 1348–1356 (1997)

[20] Petosa, A., Thirakoune, S.: Rectangular dielectric resonator antennas with enhanced gain. IEEE Transactions on Antennas and Propagation **59**(4), 1385–1389 (2011)

[21] Wu, K., Deslandes, D., Cassivi, Y.: The substrate integrated circuits-a new concept for high-frequency electronics and optoelectronics. In: 6th International Conference on Telecommunications in Modern Satellite, Cable and Broadcasting Service, 2003. TELSIKS 2003., vol. 1, p. (2003). IEEE

[22] Rayas-Sanchez, J.E., Gutierrez-Ayala, V.: A general em-based design procedure for single-layer substrate integrated waveguide interconnects with microstrip transitions. In: 2008 IEEE MTT-S International Microwave Symposium Digest, pp. 983–986 (2008). IEEE

[23] Collin, R.E.: Field Theory of Guided Waves, 2nd edn.